Acta Materialia 175 (2019) 262–275

Contents lists available at ScienceDirect

Acta Materialia

journal homepage: www.elsevier.com/locate/actamat

Intragranular localization induced by softening crystal plasticity: Analysis of slip and kink bands localization modes from high resolution FFT-simulations results

Aldo Marano [a, b], Lionel Gélébart [a, *], Samuel Forest [b]

[a] DEN- Service de Recherches Métallurgiques Appliquées, CEA, Université Paris-Saclay, F-91191, Gif-sur-Yvette, France
[b] MINES ParisTech, PSL Research University, MAT - Centre des matériaux, CNRS UMR 7633, BP 87, 9103, Evry, France

ARTICLE INFO

Article history:
Received 20 December 2018
Received in revised form
5 June 2019
Accepted 7 June 2019
Available online 12 June 2019

Keywords:
Crystal plasticity
Intragranular localization
Slip bands
Kink bands
FFT simulations

ABSTRACT

We investigate the ability of local continuum crystal plasticity theory to simulate intense slip localization at incipient plasticity observed experimentally in metals exhibiting softening mechanisms. A generic strain softening model is implemented within a massively parallel FFT solver framework to study intragranular strain localization throughout high resolution polycrystalline simulations. It is coupled to a systematic analysis strain localization modes: Equivalent plastic strain and lattice rotation fields are processed to create binary maps of slip and kink bands populations, estimate their volume fraction and mean strain level. High resolution simulations show the formation of an intragranular localization band network. The associated localization maps are used to identify accurately slip and kink bands populations and highlight the distinct evolution of kink bands, influenced by lattice rotation. Results highlight that the analysis of the nature of localization bands in numerical studies is fundamental to asses the validity of polycrystalline simulations. Indeed, it is evidenced that selection between slip or kink localization modes is only due to grain to grain incompatibilities as these two localization modes are equivalent in classical crystal plasticity models. As a result they predict the formation of a large amount of kink bands in contradiction with experimental observations of softening metals. We show that this holds for complex physics based models too. Hence, the use of classical crystal plasticity for strain localization simulation should be reconsidered in order to predict realistic localization modes.

1. Introduction

A critical issue to address in bridging the gap between microscopic mechanisms and macroscopic mechanical behavior of crystalline materials is the intrinsically heterogeneous nature of plastic slip. Several authors have provided a precise description of these discrete phenomena [1,2]: deformation occurs by formation of discrete surface steps caused by the emergence of dislocations. When intense dislocation glide occurs on a few crystallographic planes, a sharp slip localization band parallel to dislocations glide planes forms called *slip band*, widely observed in metallic single crystals and polycrystals. Another type of slip localization band observed in deformed crystals, associated with high lattice rotation and orthogonal to the glide direction, is the so-called *kink band*. Kink bands are reported in strongly anisotropic hexagonal crystals such as ice or Zinc [3–7], as a crack-tip localization mode [8–10] or for titanium alloys under high strain rate deformation [11]. Asaro and Rice bifurcation analysis [12] showed that in presence of strain softening the constitutive equations of crystal plasticity can predict both slip and kink localization modes, and a few authors have studied the formation of kink bands in crystal plasticity simulations [4,13–15].

In ductile metals, slip localization can be observed after large plastic deformation, in the form of instabilities induced by exhaustion of hardening and inhomogeneous lattice rotations. In this context, intense shear bands [16,17] and kink bands [1,18] are reported, as late deformation modes. The simulation of large deformations of polycrystals up to shear banding is possible but not addressed in the present work. By contrast, the aforementioned slip and kink bands are intended here as incipient plasticity localization modes, and are the subject of the present work.

* Corresponding author.
E-mail addresses: aldo.marano@cea.fr (A. Marano), lionel.gelebart@cea.fr (L. Gélébart), samuel.forest@mines-paristech.fr (S. Forest).

https://doi.org/10.1016/j.actamat.2019.06.010
1359-6454/

Theoretical and numerical studies have evidenced the role of local softening mechanisms in the apparition of heterogeneous deformation [19,20]. These mechanisms result of interactions between dislocations and crystal defects and are particularly intense in several metals such as irradiated or hydrogen charged polycrystals. In that case dislocation sources are locked by a hydrogen atom atmosphere making their activation much harder. Therefore required stress to generate further slip from an already active source is thought to be lower than stress needed to activate a new locked source thus promoting intense slip on a limited number of atomic planes [21,22]. Another example is the extensively studied dislocation channeling mechanism observed in a large variety of irradiated metals such as Copper [23,24], Zirconium [25,26], steel [27–30] or Vanadium [31], but also quench-hardened aluminum [32] and gold [33] single crystals. Those materials are hardened by a high density of nanometer size defects like dislocation loops or stacking fault tetrahedra. Their interaction with gliding dislocations leads to their progressive sweeping/annihilation [34] and thus to a strong local softening promoting further slip in the region where it has already occurred. Defect-free channels parallel to dislocation glide planes are indeed observed after deforming those materials, and are strongly correlated to surface slip steps indicating that defect-annihilation based softening is responsible for the formation of intense slip bands. A similar mechanism is observed in ω-enriched Ti-Nb-based gum metals where ω-particles depleted channel are correlated to surface localization bands [35]. Conversely correlation of clear channels with kink bands has never been observed and more generally kink bands are not reported as intragranular localization modes in strongly softening crystals.

Numerous efforts have been made aiming at modeling these phenomenon at the polycrystal scale as they have a first order influence on the macroscopic mechanical behavior or on cracking initiation due to localization induced stress concentrations. Relying on molecular dynamics or dislocations dynamics analyses of the dislocation channeling mechanism [36–38], many dislocation-based classical crystal plasticity models have been developed to simulate irradiated metals behavior [39–45], accounting for the softening through local defect-density dependent critical shear stress and defect-density evolution equation modeling their annihilation with increasing glide. This framework successfully reproduces the main features of macroscopic behavior of irradiated metals.

These strain softening based models have also been used to conduct full-field simulations of strain localization. Sauzay et al. [27] have explicitly modeled one or two predefined soft clear channels embedded in a hard matrix in order to study induced stress concentrations. Zhang et al. [46] have followed a different approach at the polycrystal scale by prescribing softening only on a predefined network of potential slip bands in 2D polycrystalline FE simulations. This modeling strategy allows localization bands to form but requires prior knowledge of geometric characteristics of the bands network. On the contrary, Erinosho and Dunne [47] have modeled a full 3D polycrystal with a strain softening behavior with no assumptions on localization paths. Their simulations predict formation of transgranular localization bands due to slip softening, however they used cubic grains microstructure and associated mesh resolution (average of 1000 elements per grain) is too coarse to reproduce accurately intragranular slip localization. Patra and McDowell [48,49] have recently published simulations with higher resolution using a dislocation channeling based softening model, and their results predict indeed formation of intragranular localization bands. However they simulated a 2D aggregate under the generalized plane strain hypothesis which is not representative of complex localization patterns that can arise in 3D microstructures. Most importantly, they did not analyze the slip or kink nature of the simulated bands in order to compare results with experimentally observed cleared channels in irradiated steels.

In general, the analysis of plastic localization modes is overlooked in numerical studies of strain localization in polycrystals. Yet, slip or kink banding are observed in distinct materials and have different characteristics. Thus, it is fundamental to examine the nature of localization bands predicted by crystal plasticity models to assess their validity. This work aims at gaining deeper insight into the ability of softening classical crystal plasticity to simulate accurately intense intragranular localization observed in the various metals exhibiting softening mechanisms. To this end, we implemented a generic softening crystal plasticity model within a massively parallel FFT solver allowing to model three dimensional polycrystalline unit cells with higher grid resolutions and number of grains. A systematic analysis of simulated localization bands is carried out on simulations results. For that purpose, we developed a methodology using full-field outputs of the FFT simulations to build localization mode maps that allow to identify and quantify simulated slip and kink bands populations. We study the influence of mechanical behavior, crystal structure and various simulation parameter on localization. Then we discuss the bands formation process in classical crystal plasticity simulations, and show that they systematically lead to comparable amount of slip and kinks bands. Finally, we compare the results of our generic analysis with a state of the art physics based model of irradiated austenitic stainless steel.

2. Crystal plasticity constitutive model

The constitutive model used in this study reduces to the two main ingredients allowing to simulate strain localization along crystallographic planes: the classical finite deformation crystal plasticity framework combined with a softening flow rule. This simple and generic formulation allows to avoid any material complexity to focus the study on the link between strain softening crystal plasticity and slip localization. Crystal plasticity kinematics is described by the classical multiplicative decomposition of the deformation gradient tensor $\boldsymbol{F}$ into its elastic part $\boldsymbol{F_e}$ and its plastic part $\boldsymbol{F_p}$ [50]: $\boldsymbol{F} = \boldsymbol{F_e}\cdot\boldsymbol{F_p}$. where $\boldsymbol{F_p}$ maps the reference configuration to the isoclinic stress-free local configuration where crystal lattice orientation is unchanged with respect to the reference configuration and $\boldsymbol{F_e}$ maps the intermediate local configuration into the deformed configuration, describing crystal lattice distortion and rotation. It is assumed that plastic deformation takes place through the slip of dislocations on prescribed slip planes with normal $\boldsymbol{n}^\alpha$ along slip direction $\boldsymbol{m}^\alpha$. The plastic velocity gradient $\boldsymbol{L}_p = \dot{\boldsymbol{F}}_{\boldsymbol{p}}\cdot\boldsymbol{F}_{\boldsymbol{p}}^{-1}$ is then determined by the shearing rate of the N_s material slip systems through the relation:

$$\boldsymbol{L}_p = \sum_{s}^{N_s} \dot{\gamma}^\alpha \boldsymbol{\mu}^\alpha \tag{1}$$

where γ^α is the plastic slip on slip system α and $\boldsymbol{\mu}^\alpha = \boldsymbol{m}^\alpha \otimes \boldsymbol{n}^\alpha$ the Schmid tensor for slip system α. Crystal elasticity is defined by a linear relation between the Green-Lagrange elastic strain tensor $\boldsymbol{E}_e = \frac{1}{2}(\boldsymbol{F}_{\boldsymbol{e}}^T\cdot\boldsymbol{F_e} - 1)$ and Piola elastic stress tensor $\boldsymbol{\Pi}_e = det(\boldsymbol{F_e})\boldsymbol{F}_{\boldsymbol{e}}^{-1}\cdot\boldsymbol{\sigma}\cdot\boldsymbol{F}_{\boldsymbol{e}}^{-T}$ (defined in the isoclinic configuration): $\boldsymbol{\Pi}_e = \underline{\underline{\boldsymbol{\Lambda}}} : \boldsymbol{E}_e$. $\underline{\underline{\boldsymbol{\Lambda}}}$ is the fourth-order elastic tensor, $\boldsymbol{\sigma}$ the Cauchy stress tensor w.r.t. current configuration. Plastic flow is described by a Norton-type visco-plastic flow rule (Eq. (2)) and an exponential softening of critical resolved shear stress τ_c^α with increasing cumulated slip on each slip system γ_{cum}^α (Eq. (4)).

$$\dot{\gamma}^\alpha = \left\langle \frac{|\tau^\alpha| - \tau_c^\alpha}{K} \right\rangle^n \mathrm{sgn}(\tau^\alpha) \tag{2}$$

$$\tau^{\alpha} = \boldsymbol{M} : \boldsymbol{\mu}^{\boldsymbol{\alpha}} \tag{3}$$

$$\tau_c^{\alpha} = \tau_{c_i}^{\alpha} - \Delta\tau^{\alpha}\left(1 - \exp\left(-\frac{\gamma_{cum}^{\alpha}}{\gamma_0^{\alpha}}\right)\right) \tag{4}$$

Resolved shear stress τ^{α}, is calculated by the projection of the Mandel stress tensor $\boldsymbol{M} = \det(\boldsymbol{F_e})\boldsymbol{F_e}^T \cdot \boldsymbol{\sigma} \cdot \boldsymbol{F_e}^{-T}$ on slip system α (Eq. (3)). n and K are Norton-law parameters. The model involves three important material coefficients: τ_{c_i}, $\Delta\tau^{\alpha}$ are respectively the initial critical shear stress and the maximum softening that can be reached on slip system α, and γ_0^{α} is a parameter adjusting the softening rate.

Despite its simplicity, we believe it to be representative of most softening models for irradiated metals [39–45,51]. They are indeed formulated within the same kinematic framework and rely on softening rules that, when written in the case of single slip, reduce to the an exponential decay of the critical resolved shear stress similar to Eq. (4). Appendix A detailed calculation is provided in A to support this argument.

3. Slip/kink localization modes analysis

In this section, we present a post processing methodology designed to identify the nature of localization bands in FFT simulations results. In order to identify localization bands, we use the equivalent plastic strain field defined by Eq. (6) as a measure of local slip intensity. Contrary to slip bands, kink bands involve high lattice rotation that can be used to distinguish kinks from slip bands. Lattice rotation angle is computed using the polar decomposition of the elastic part of the deformation gradient: $\boldsymbol{F_e} = \boldsymbol{R_e} \cdot \boldsymbol{U_e}$. Neglecting the small elastic distortion described by the right stretch tensor $\boldsymbol{U_e}$, the elastic rotation tensor $\boldsymbol{R_e}$ is interpreted as the lattice rotation and the corresponding angle θ can be computed with Eq. (5). p is the cumulative plastic strain.

$$\theta = \arccos\left(\frac{1}{2}\left(\mathrm{tr}(\boldsymbol{R}^e) - 1\right)\right) \tag{5}$$

$$p = \int_0^t \sqrt{\boldsymbol{L}_p : \boldsymbol{L}_p}\, dt \tag{6}$$

These fields are then used to define L and R, indicator functions respectively of slip localization and high lattice rotation areas, by the relations:

$$L(\boldsymbol{X}) = \mathscr{H}(P(\boldsymbol{X}) - \overline{p}\Phi_D) \tag{7}$$

$$R(\boldsymbol{X}) = \mathscr{H}(\theta(\boldsymbol{X}) - \overline{\theta}\Phi_R) \tag{8}$$

where $\mathscr{H}$ is the Heaviside step function and $\boldsymbol{X}$ is the material point coordinate vector. They indicate regions where fields p and θ are above a level defined by their mean value $\overline{p}$ and $\overline{\theta}$ over the whole unit cell multiplied by suitably chosen relative thresholds, Φ_D and Φ_R respectively. Therefore L maps plastic strain localization areas that are mainly the localization bands.

The definition of a kink band provided by Asaro and Rice [12] is a localization band perpendicular to the slip plane. Localization of plastic slip along the normal to the slip plane mechanically induces lattice rotation. As discussed in the introductory section, observed kink bands are always associated to lattice rotation. This suggests a practical definition of kink bands in simulations results as areas exhibiting both intense plastic slip and high lattice rotation, that is to say $L(\boldsymbol{X}) = 1$ and $R(\boldsymbol{X}) = 1$. We then assume that localization area without intense lattice rotation are slip bands. Hence, kink and slip bands indicator functions, S and K, are given by:

$$K(\boldsymbol{X}) = L(\boldsymbol{X}) \cdot R(\boldsymbol{X}) \tag{9}$$

$$S(\boldsymbol{X}) = L(\boldsymbol{X}) - K(\boldsymbol{X}) \tag{10}$$

and can be plotted simultaneously to evidence localization modes. Finally, these functions are used to determine for the slip and kink bands population, volume fractions, f_S and f_K, and mean value of equivalent plastic strain, $<P_S>$ and $<P_K>$, as follows:

$$<P_K> = \frac{1}{f_K V}\int_{\Omega} K(\boldsymbol{X})P(\boldsymbol{X})\boldsymbol{dX} \tag{11}$$

$$<P_S> = \frac{1}{f_S V}\int_{\Omega} S(\boldsymbol{X})P(\boldsymbol{X})\boldsymbol{dX} \tag{12}$$

4. FFT simulations

Simulations are performed using the FFT solver AMITEX_FFTP[1] which offers two main advantages. First, its massively parallel implementation enables to simulate strain localization in three dimensional and high resolution polycrystalline unit cells in order to overcome limitations observed in the literature. Previous simulations aiming at modeling softening induced strain localization where indeed conducted either on 3D microstructures but with low resolutions [47] or with high resolution but 2D microstructures [49]. Second, FFT based methods provide mechanical fields in the form of 3D images very well suited for the computation of localization modes indicator functions and associated quantities defined in the former section.

4.1. Numerical implementation

The FFT solver AMITEX is based on the original fixed-point numerical scheme proposed by Moulinec and Suquet [52] but implements a modified discrete Green operator based on a finite difference method to evaluate derivatives in Fourier space, equivalent to the one proposed by Willot [53]. This numerical scheme is shown to be equivalent to the use of hexahedral finite elements with reduced integration [54]. In addition, Anderson's convergence acceleration technique is applied to the fixed point algorithm [55–57].

Material constitutive law is integrated using a fully implicit θ-method implementation of constitutive equations generated by the MFront code generator [58]. Internal variables increments $\{\Delta\boldsymbol{E}_e, \Delta\gamma^{\alpha}\}$ between time t and $t + \Delta t$ are computed from their value at time t $\{\Delta\boldsymbol{E}_e^t, \gamma^{\alpha,t}\}$ by solving with Newton-Raphson algorithm the following system of non linear equations:

$$\Delta\boldsymbol{E}_e + \boldsymbol{E}_e^t - \frac{1}{2}\left(\boldsymbol{F_e}^{T,t} \cdot \boldsymbol{F_e}^t - 1\right) = 0 \tag{13}$$

$$\Delta\gamma^{\alpha} - \left\langle \frac{|\tau^{\alpha}| - \tau_c^{\alpha}}{K} \right\rangle^n sgn(\tau^{\alpha})\Delta t = 0 \tag{14}$$

Note that here Green-Lagrange elastic strain $\boldsymbol{E}_e$ tensor is

[1] http://www.maisondelasimulation.fr/projects/amitex/html/.

considered as an additional variable to avoid inaccuracies in numerical evaluation of $\boldsymbol{F_e}$, following the approach presented in Ling et al. [59].

4.2. Simulations description

FFT simulations apply periodic boundary conditions to 3D regular grids of voxels (i.e. 3D images). Two types of polycrystalline microstructures have been generated using voxelized periodic Voronoi tessellations:

- 2D periodic unit cells (1 voxel thick in the X direction) containing 225 grains (15^2). Because of X direction periodicity, this is equivalent to 3D infinite columnar grains in the X direction, also equivalent to a 2D modeling under generalized plane strain hypothesis. One in plane slip system is modeled, and each grain is assign a random 2D orientation, leaving all slip plane normals and glide directions in the (Y,Z) plane.
- 3D periodic unit cells consisting of 64 grains (4^3) with random grain orientations. In order to assess results variability, 9 realizations of these random microstructures have been employed, as well as a 512 grains (8^3) random aggregate. Simulations have been carried out using the 12 FCC slip systems $\{111\}<110>$, the 12 BCC slip systems $\{110\}<111>$ or the 3 basal HCP slip systems $\{0001\}<1\bar{2}10>$.

Unless otherwise stated grid resolution has been chosen so that mean grain size is resolved by 50 voxels. Thus, 2D and 3D simulations contain in average respectively 2500 and 125000 voxels per grain.

In addition to periodic boundary conditions, tensile loading is applied in the Z direction by prescribing the mean value of the corresponding component of the displacement gradient $\boldsymbol{H} = \boldsymbol{F} - 1$ at a constant strain rate of $10^{-5}\ s^{-1}$. Mean values of all other components of engineering stress (first Piola-Kirchhoff stress) are prescribed to zero.

Table 1
Material parameters used for all simulations.

K	n	E	ν	τ_{C_i}	τ_{C_f}	γ_0
$\frac{1}{10\ \text{MPa}.s^{\overline{n}}}$	15	100000 MPa	0.3	100 MPa	80 MPa	0.1

Constitutive model parameters used in all simulations unless otherwise stated are listed in Table 1. All simulations feature isotropic linear elasticity. Norton law coefficients n and K values are chosen in order to limit rate dependence without damaging numerical convergence. As simulated crystal systems have only one family of equivalent slip systems, superscript α on flow rule parameter is omitted in the rest of this paper. The single slip system softening behavior and simulated macroscopic mechanical behavior for 2D, 3D FCC and 3D BCC polycrystals are plotted on Fig. 1 for this set of material parameters which involves 20% maximum softening of the critical resolved shear stress on each slip system.

5. Results

5.1. Identification of slip and kink bands

Fig. 2(a and b) shows equivalent plastic strain and lattice rotation fields simulated for the 2D microstructure after 1% overall elongation. Clear networks of intragranular slip localization bands have formed as well as intense lattice rotation bands. Indicator functions S and K of slip/kink bands are computed from these fields as defined in sec. 3. They are plotted respectively in red/blue and superposed to the microstructure in order to construct the associated localization mode map (c). In addition, slip planes traces are superposed to compare the detected slip and kink band orientations to crystallographic directions. The zoomed view (d) clearly demonstrates that all red/blue bands are respectively parallel/perpendicular to a slip plane. Fig. 3 shows similar results for a 3D simulation of a FCC polycrystal, as well as the video provided as supplementary material.

Supplementary video related to this article can be found at https://doi.org/10.1016/j.actamat.2019.06.010.

A systematic study of simulated bands confirms that this correspondence holds for most detected bands. The proposed methodology provides then an efficient tool to identify plastic localization modes that could be applied to any finite strain crystal plasticity based simulation. It is especially helpful to analyze 3D simulations (see. Fig. 3) which lead to complex 3D images of dense planar bands network, making direct observation of bands orientation cumbersome.

Thresholds detection values have been tuned by hand to obtain

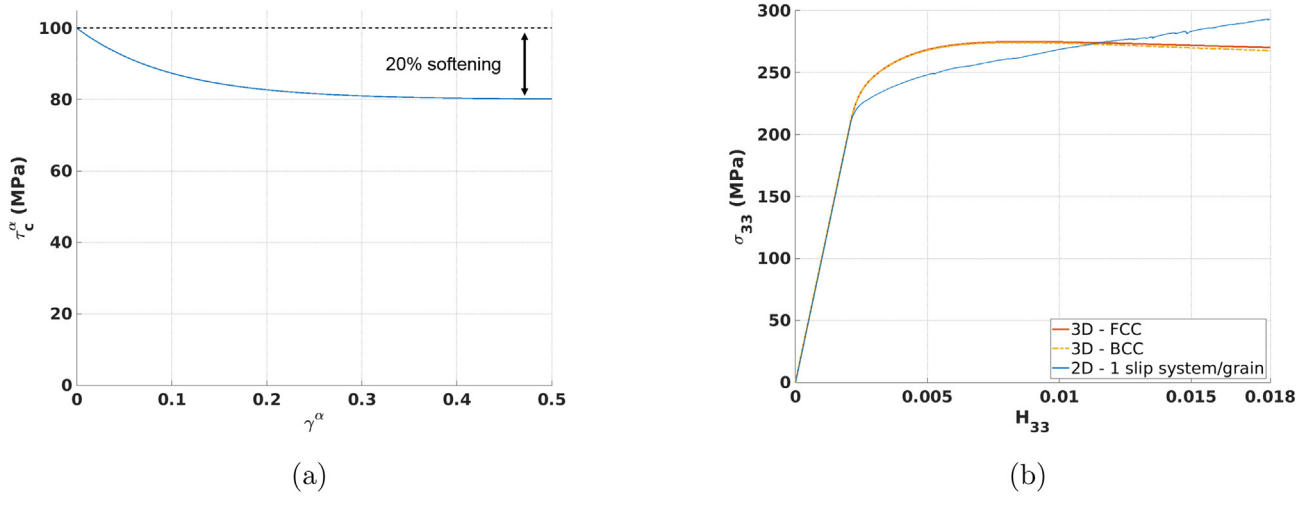

Fig. 1. Critical resolved shear stress evolution curve used for all simulations (a), and associated macroscopic stress-strain responses for different polycrystalline simulations (b) (FCC and BCC curves are almost superimposed).

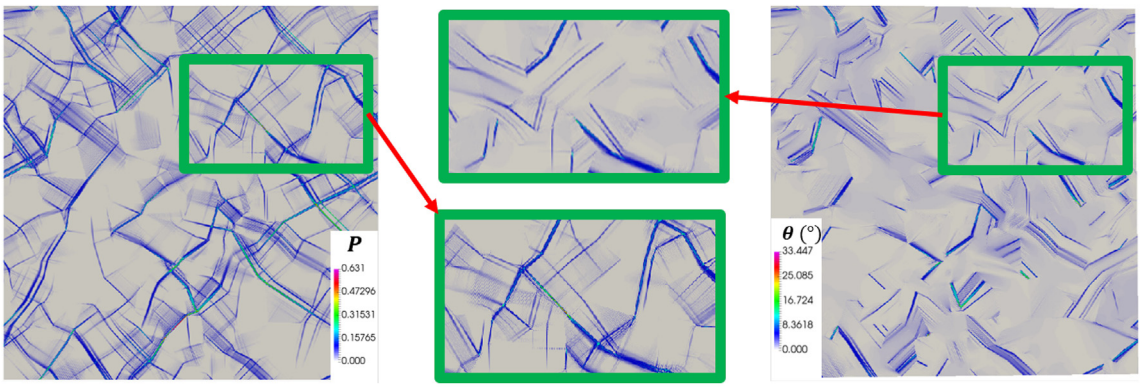

(a)

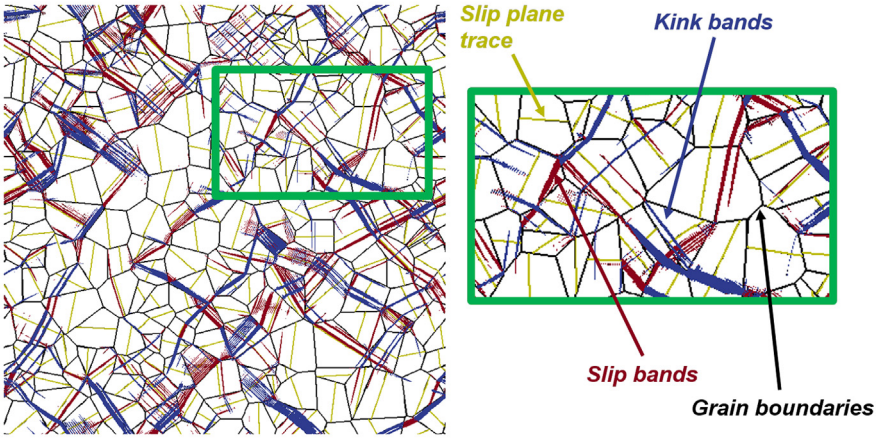

(b) (c)

Fig. 2. Equivalent plastic strain (a) and lattice rotation angle (b) fields for the 2D polycrystal (1 in-plane slip systems) after 1% overall strain. Associated localization map (c). Slip (red) and kink (blue) bands are always respectively parallel/orthogonal to a slip plane (yellow) as illustrated by the zoom at the green-surrounded region (d). Grain boundaries are represented by black lines. Grid resolution: 750 × 750 voxels. (For interpretation of the references to colour in this figure legend, the reader is referred to the Web version of this article.)

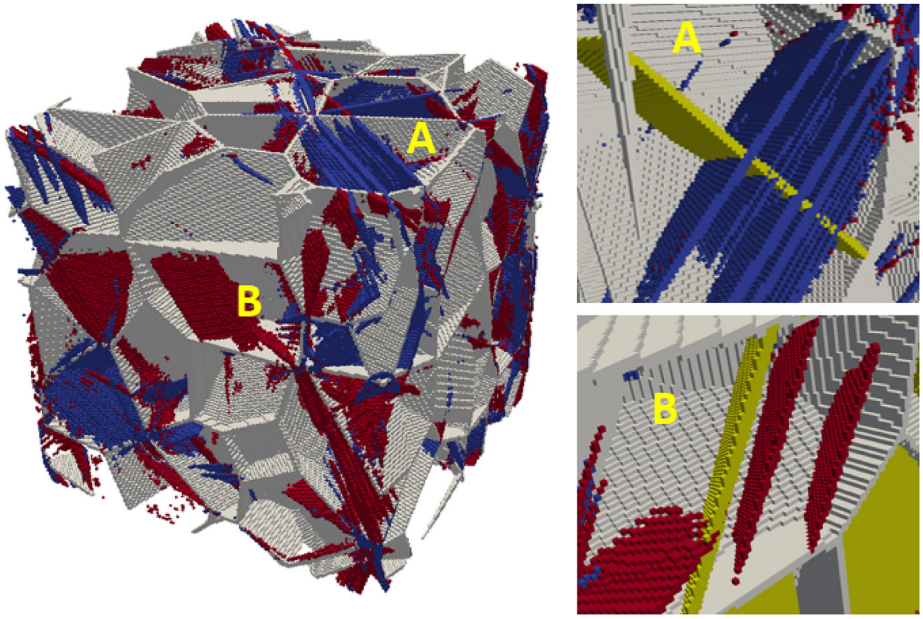

Fig. 3. Localization map built for a FCC 3D polycrystal after 2% overall strain showing slip/kink bands (red/blue) and grain boundaries (grey). Activated slip plane (yellow) is plotted on the zooms on A and B marked grains. The A grain contains a series of kink bands orthogonal to the activated slip plane. The B grain contains 2 slip bands parallel to the activated slip plane. Grid resolution: 200 × 200 × 200 voxels. (For interpretation of the references to colour in this figure legend, the reader is referred to the Web version of this article.)

optimal maps. Too low values of Φ_D leads to detection of more homogeneously deformed area whereas too high values leads to the detection of only a few localization bands. Best compromise has been achieved for $\Phi_D = 3$. Φ_R is then chosen to obtain best optimal band separation. Too high values lead to identification of kinks exhibiting too low lattice rotation as slips. Besides, regions with a slight inhomogeneous deformation can also have a moderate local lattice rotation and a slip band crossing them would be identified as a kink for too low values of Φ_R. Optimal results have been obtained for $\Phi_R = 2$. Thresholds values do not have a strong impact on qualitative analysis of localization maps. However they have a stronger influence on bands volume fraction and mean plastic strain estimation. Yet using the same set of threshold values to analyze different simulations allows for relative comparison of these quantities that provides qualitative insights on strain localization properties, as presented in the following sections.

5.2. Grid resolution influence on slip and kink bands

Fig. 4 shows the evolution of slip and kink band volume fractions and mean plastic strain after 1% total elongation for 2D simulations conducted with increasing grid resolution. When increasing grid resolution, slip and kink bands volume fraction decreases and their mean strain level increases. Softening material behavior is known to induce numerical instabilities leading to such mesh dependence. However, results show that kink bands properties are less sensitive to grid resolution. Associated localization maps illustrate this trend: when increasing grid resolution the slip bands thickness decreases while their number increases. In contrast kink bands patterns are more similar in the three maps.

Due to lattice rotation, the Schmid factor in kink bands can be locally decreased (or the reverse) and hinder further slip. Hence, lattice rotation hardening restrain slip localization. This rotation induced hardening mechanism opposes to material softening and can explain why kink bands population exhibit a lower mesh size dependance despite the strongly softening material behavior.

5.3. Softening influence on slip and kink bands

Fig. 5(a and b) presents the evolution of slip/kink volume fractions and mean plastic strain after 1% total elongation when varying the maximum softening level $\Delta\tau$ for 2D simulations. Again, slip and kink band population evolutions present significant differences. Increasing $\Delta\tau$ causes bands volume fraction to decrease, slightly more for slip bands. The mean plastic strain level increases with softening intensity for both populations but increase is steeper for slip bands. Associated localization maps Fig. 5(e and f) show that softening decreases bands thickness and increases they number, with a stronger influence on slip bands pattern than kink bands.

Softening will also promote increased plastic slip in kink bands but because of rotation induced hardening, slip localization will be hindered and additional plastic slip will occur by widening of existing kink bands. This mechanism explains the smaller increase/decrease in kink bands mean plastic strain/volume fraction for a higher $\Delta\tau$.

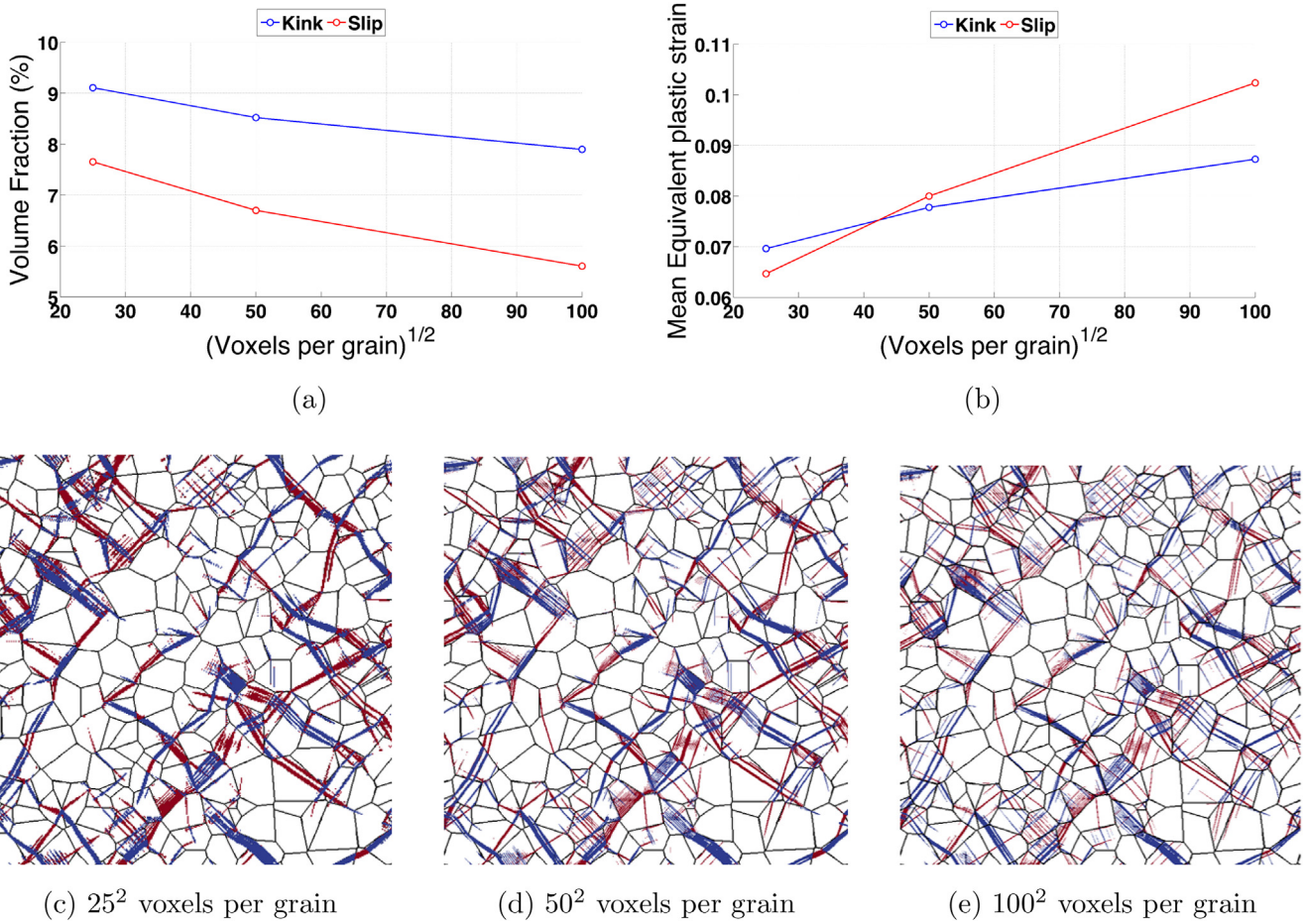

Fig. 4. Influence of grid resolution on slip (red) and kink (blue) bands volume fraction (a) and mean equivalent plastic strain (b) for the 2D polycrystal after 1% overall strain. (c–e): associated localization maps. (For interpretation of the references to colour in this figure legend, the reader is referred to the Web version of this article.)

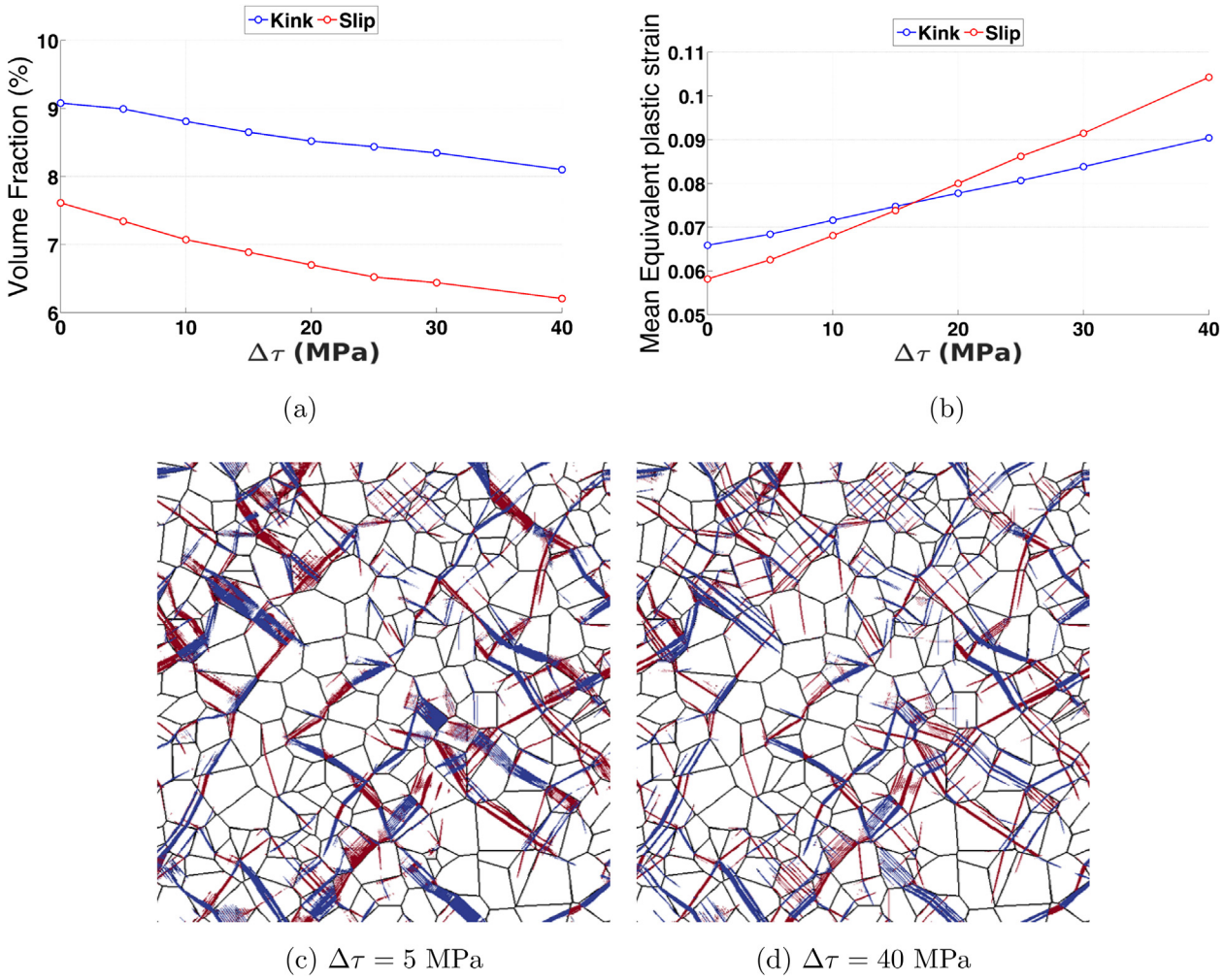

Fig. 5. Evolution of slip/kink bands volume fraction (a) and mean equivalent plastic strain (b) with softening intensity for the 2D polycrystal after 1% overall strain. Selected localization maps are plotted for specific values of softening intensity (c–d). Grid resolution: 750×750 voxels.

5.4. Comparison between 2D and 3D simulations

Fig. 6 and Fig. 7 show the evolution of slip/kink band volume fractions and mean plastic strain level with increasing loading for a 2D simulation and a 3D simulation of a FCC polycrystal. In both simulations, the volume fraction grows more quickly for kinks than slip bands. 2D localization map snapshots on Fig. 6 (a) show that kink bands volume fraction increases mainly because of widening of existing bands whereas increase in slip bands volume fraction is mostly due to new bands formation. Conversely the difference in slip/kink band thickness observed on 3D localization map snapshots is smaller Fig. 6 (b). On the other hand, Fig. 7 evidences that slip/kink mean plastic strain levels are almost identical in the two cases.

For geometrical reasons, the same amount of lattice rotation induces lower variation of Schmid factor in three dimensional simulations compared to the 2D simulations where all directions involved in Schmid factor calculations (glide direction, slip plane normal and loading directions) are coplanar. Hence, lattice rotation induced hardening should have a minor impact in 3D simulations than in 2D simulations, which is consistent with actual results: stronger lattice rotation will induce stronger widening of kink bands in the 2D case as overall strain increases.

5.5. Sensitivity to simulated volume element

To our knowledge, kink bands have never been reported for strongly softening metals. However, the results presented in previous sections reveal large proportions of kinks in simulated localization band networks. In order to find out if these proportions are due to the specific microstructure of the used unit cell, 9 random realizations of a 64 grain and one 512 grain 3D polycrystals have been generated to characterize the variability of simulated localization bands populations with volume element instances, and volume element size. Fig. 8 presents the evolution of slip/kink bands volume fraction with increasing loading. It is found that for the 64 grains volume element the standard deviation of simulated band volume fractions is generally smaller than the difference between slip and kink bands volume fractions. Results of the 512 grain aggregate simulation are contained within the error bars, very close to the mean value of the 9×64 grains simulations. Besides, similar localization networks are observed on 64 and 512 grains simulations localization maps. It follows that a single 64 grains volume element may be sufficient to draw a qualitative analysis of slip/kink bands populations for these cubic crystals.

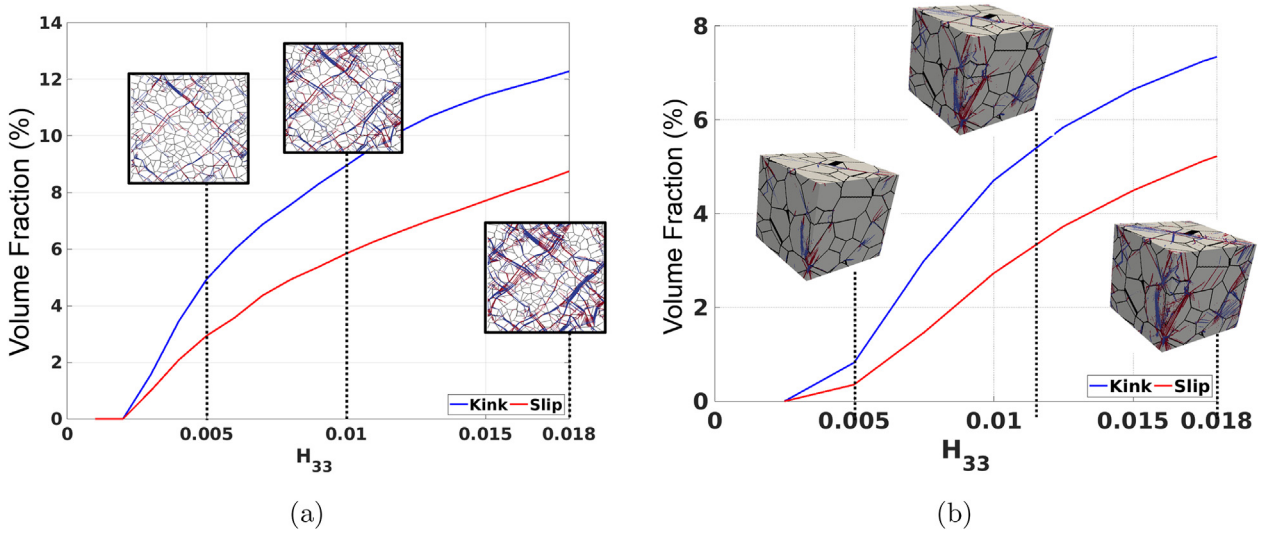

Fig. 6. Evolution of slip/kink band volume fraction for the 2D simulation (a) and a FCC 3D polycrystal (b), with snapshots of associated localization maps.

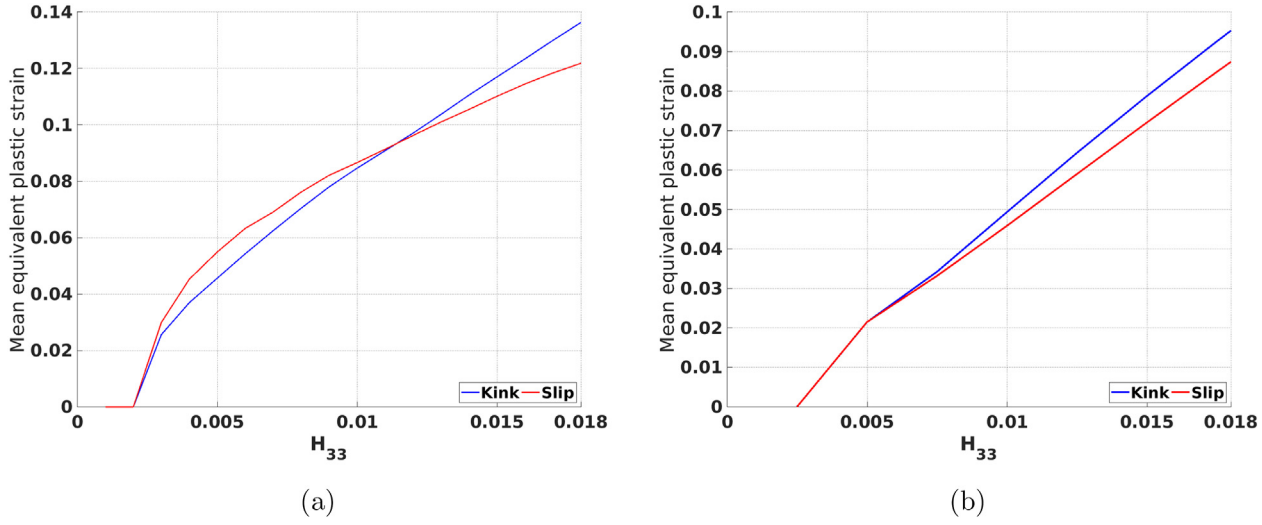

Fig. 7. Evolution of slip/kink band mean equivalent plastic strain for the 2D (a) and a FCC 3D 64 grain polycrystal (b).

6. Discussion

6.1. Localization bands formation in crystal plasticity simulations

Asaro and Rice [12] have shown that both slip and kink bands arise as the two possible bifurcation modes for elasto-plastic single crystals undergoing single slip at large strains. They defined this two modes as slip localization planes respectively orthogonal to glide plane normal direction $\boldsymbol{n}$ (slip bands) and glide direction $\boldsymbol{m}$ (kink bands). In the case of strain-softening crystals, their analysis shows that both modes become simultaneously possible at incipient plasticity. Incipient plasticity always occurs at small strain in metallic materials and in these conditions small strain formulation of crystal plasticity equations are valid to describe material behavior. In the small strain framework, resolved shear stress τ^α on slip system α and plastic strain are computed as follow:

$$\tau^\alpha = \boldsymbol{m}\cdot\boldsymbol{\sigma}\cdot\boldsymbol{n} \tag{15}$$

$$\dot{\varepsilon}_p = \sum \alpha\dot{\gamma}^\alpha \boldsymbol{m}\otimes_{sym}\boldsymbol{n} \tag{16}$$

The Cauchy stress $\boldsymbol{\sigma}$ being a symmetric tensor and $\otimes_{sym}$ the symmetric tensor product, $\boldsymbol{m}$ and $\boldsymbol{n}$ play a perfectly symmetric role in Eq. (15): Inverting them leaves the equation unchanged. This consideration implies that kink and slip bifurcation modes are strictly equivalent at incipient plasticity with respect to the constitutive equations. It follows that structural effects, i.e. grain to grain plastic strain incompatibilities will govern the selection of slip or kink localization modes.

In order to provide an illustration of this property, two simulations have been carried out using the same grain geometry, grain orientations and material coefficients, but using two distinct crystal slip systems: the 12 FCC $\{111\}<110>$ slip systems and the 12 BCC $\{110\}<111>$ slip systems. The latter are indeed obtained by switching slip planes normals and glide directions of the FCC slip systems, thus according to Asaro and Rice analysis the potential localizations planes are the same in both polycrystals. The two identical microstructures induce identical structural effects and

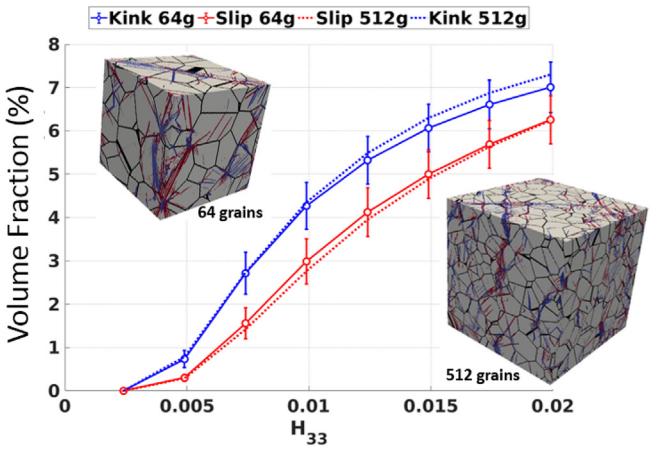

Fig. 8. Slip/kink bands volume fraction evolution with loading in FCC polycrystal. Plotted value is the mean of 9 realizations of a 64 grains random Voronoi aggregate, error bars indicating standard deviation of the 9 simulations. Results for the 512 grains random Voronoi aggregate are plotted in dashed-lines. Associated localization maps show localization at 2% overall strain in one 64 grains polycrystal and in the 512 grains one.

thus should activate the same localization planes at incipient plasticity. Simulations results clearly illustrate this point: In corresponding localization maps, shown on Fig. 9, most of FCC slip (resp. kink) bands have a kink (resp. slip) counterpart for the BCC crystal structure. Then, finite strain kinematics leads to distinct evolutions of slip and kink bands because of rotation induced hardening, discussed in previous sections. It explains why the two localization maps are not strictly equivalent after applying 1% overall tensile strain.

With a the view to investigating the influence of structural effects on slip/kink band formation a simulation has been carried out for a HCP crystal considering only the 3 basal slip systems $\{0001\}<1\bar{2}10>$. In that case the distribution of available localization planes is then strongly anisotropic and should be more influenced by structural effects than in more isotropic cases such as cubic crystals. Indeed, the only potential plane for slip band formation in each grain is the basal plane, whereas kink banding, in prismatic planes offer 3 times more planes to accommodate grain to grain plastic incompatibilities. Fig. 10-a shows that kink bands volume fraction is approximately two times higher than slip band volume fraction, whereas the two quantities are much closer for the FCC crystals (Fig. 8). Associated localization map (Fig. 10-c) shows that localization occurs mainly at grain boundary triple lines from which kink bands seem to emerge more often than slip bands.

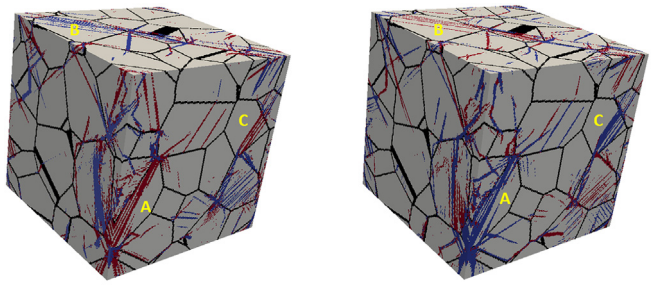

(a) FCC (b) BCC

Fig. 9. Localization maps of 3D polycrystals after loading to 1% strain with (a): 12 FCC slip systems {111}[110] and (b) 12 BCC slip systems {110}[111], with identical geometry and grains orientations. Grains marked A,B and C illustrate the almost identical band structure, with FCC slip banding (resp. kink) corresponding to BCC kink banding (resp. slip). $200 \times 200 \times 200$ voxels.

Triple lines grain boundary induce strong stress concentrations due to grain to grain incompatibilities. They are highly likely to trigger strain localization in some or all of the neighboring grains. Thus this structural effect will promote localization paths that extend over at least 2 grains and cross grain boundaries close to triple lines. Considering that geometrically there are three distinct kink planes against only one slip plane, the probability to form such transgranular localization paths across kink bands is higher. This could explain why the gap between slip and kink bands volume fractions is higher in the case of the simulated HCP crystal. It is also interesting to note that in this case the intensity of kink bands is slightly higher and shows a steeper growth compared to slip bands after approximately 1.5% strain (Fig. 10-b), which is not observed for the FCC structure (with the same set of material coefficients, microstructure and grid resolution).

6.2. General validity of the bands formation mechanism for classical crystal plasticity models

This study is based on a simple generic softening constitutive model. However, strain localization in crystals is strongly dependent on factors such as strain hardening, strain-rate sensitivity, the complex interactions between dislocations of different slip systems, and of dislocations with other crystal defects. All those can be accounted for in the classical crystal plasticity (CCP) framework through the formulation of the constitutive equations that govern material behavior. The purpose of this section is to demonstrate that the bands formation mechanisms, resulting in comparable amounts of slip and kink bands, and revealed by our generic analysis, is also valid for complex physics-based models.

Our generic model with an additional linear hardening term (Appendix B) allows to study the impact of varying the softening/hardening rate and strain-rate sensitivity affecting each slip system independently. Simulations obtained for various softening intensity are described in subsection 5.3. Appendix B presents results for different material strain-rate sensitivity and a single slightly hardening simulations. All show very similar localization pattern: the constitutive behavior has an influence on the number, the thickness and the intensity of the bands but not on the localization modes observed in the grains.

Multi-scale CCP models encompass the complex interactions mechanisms between dislocations of various slip systems, and crystal defects, that yield a more realistic softening behavior. Despite this complexity, once softening occurs, slip will localize indifferently through slip or kink banding in order to best accommodate strain. Then, the relative amount of simulated kink and slip bands should remain unchanged.

In order to verify this prediction, we have carried out a simulation using a physics-based state of the art model of irradiated austenitic stainless steel, described in Ref. [45]. It features the modeling of the dislocation density on each slip of the twelve slip systems, the density of each of the four family of defect loops, a detailed modeling of the interactions between dislocations and loops, and between slip systems. It accounts for the annihilation of loops by gliding dislocation, yielding strong softening on several slip systems.

We have reported in Fig. 11 the results of this simulation and one carried out with our generic softening model, with same loading and FCC microstructure. Careful comparison of both localization maps reveals that the band pattern obtained with the state of the art model (a) encompasses the one obtained with the generic model (b). It proves that the same structural effects yield the same localization modes in the same grains even for two very different CPP models. The band pattern is more complex but it is clear on the map (a) that the relative amount of kink and slip bands is roughly the same than in map (b).

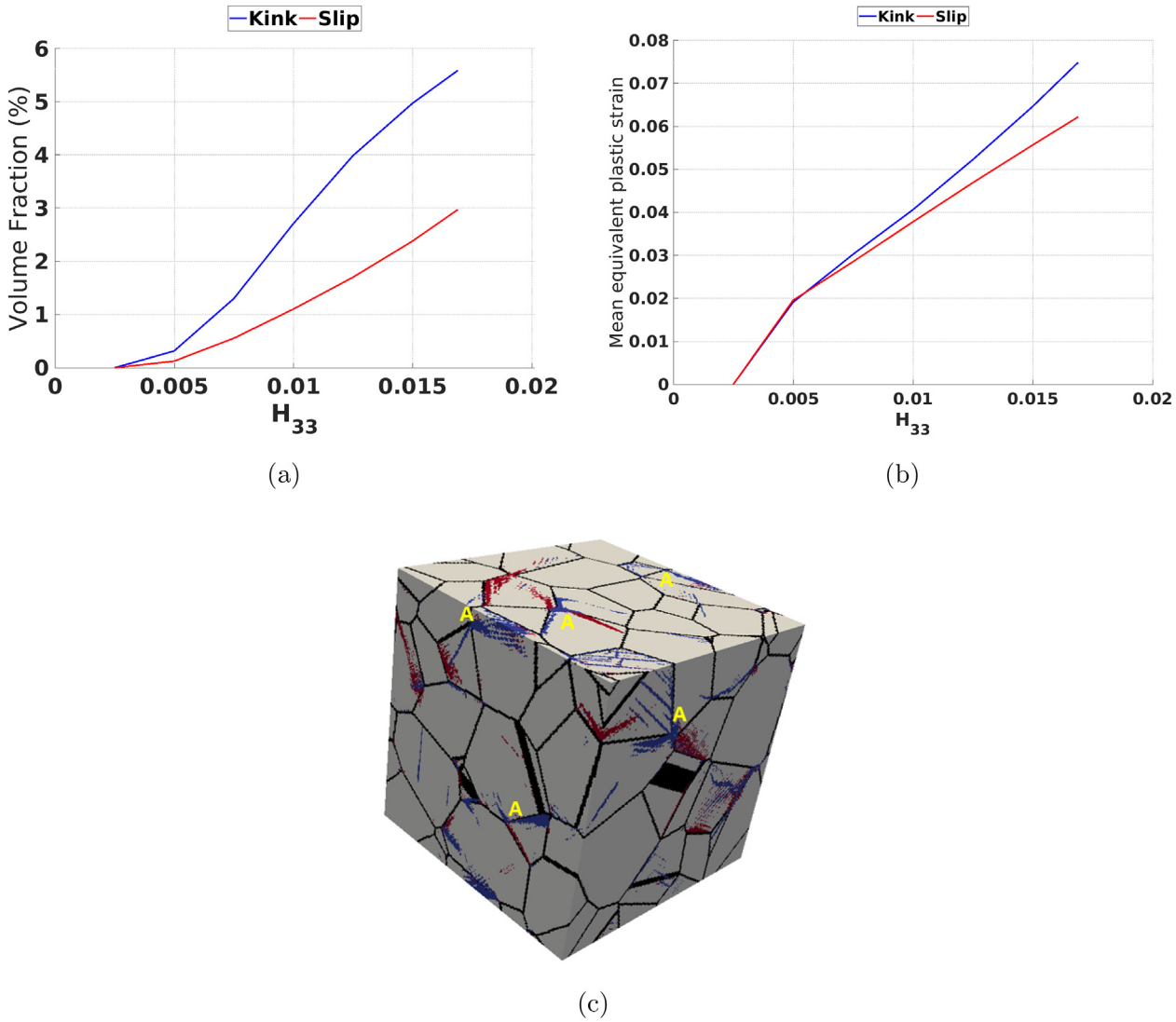

Fig. 10. Slip/kink bands volume fraction evolution (a) and mean equivalent plastic strain (b) for a 64 grains random HCP polycrystal. Zones marked A in the associated localization map after 1% overall strain (c) show that localization occurs generally at triple grain boundary junctions mostly through kink banding.

This investigation confirms the validity of the localization modes formation mechanism discussed in subsection 6.1 for all set of constitutive equations relying on softening CCP. They can strongly affect the characteristics of the bands (number, thickness, intensity) but do not affect the selection of slip or kink banding, which are only determined by the crystal structure and structural effects. Thus, despite being detailed description of physical mechanisms, CCP will systematically induce formation of comparable amounts of slip and kink bands.

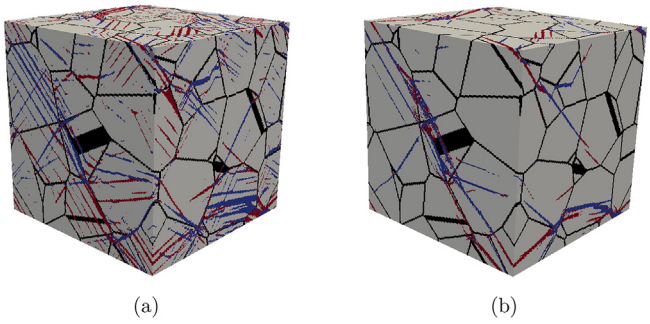

Fig. 11. Localization maps of FC 3D polycrystals after loading to 1% strain obtained with a state of the art crystal plasticity model of austenitic stainless steel [45] (a) and the generic model with strong softening ($\Delta\tau = 50$ MPa) (b). $200 \times 200 \times 200$ voxels.

It must be noted that for all models considered here, initial single crystal domains (i.e. grains in polycrystalline simulations) are considered homogeneous regarding material properties, which is standard for polycrystalline crystal plasticity simulations in the literature. Asaro and Rice's analysis relies on the study of a bifurcation occurring in an homogeneous single crystal continuum. Hence, our results confirm and extend Asaro and Rice's analytical results for such CCP polycrystalline simulations.

6.3. Critical assessment of classical crystal plasticity models use for strain localization simulation

Lebensohn et al. [14] carried out crystal plasticity simulations of ice HCP polycrystals deforming mainly through basal slip. As in our HCP simulation, they note significant occurrence of intense kink bands in their results which is also in agreement with reported observations of kink bands in ice [3,4]. Flouriot et al. [60] have noted kink bands formation in crack-tip field simulations in a FCC

crystal that are similar to those observed with crack-tip field measurements in ductile crystals [9]. As in this two situations, kink bands observations are mostly reported where strong strain incompatibilities arise such as crack-tip fields, compression of HCP single crystals [6] or deformation of strongly anisotropic HCP polycrystals [3,4,7] mainly deforming through basal slip. In those cases, crystal plasticity models appears to be well-suited to simulate their formation.

However, the case of irradiated Zirconium polycrystals provides a good example to also highlight their limitations. They are HCP crystals deforming mainly through basal slip and could exhibit formation of kink bands, like ice polycrystals, because of this slip anisotropy. On the contrary, deformed Zr polycrystal observations reveal only very intense slip bands, associated to dislocation channeling, a strongly softening mechanism, while kink bands have never been reported yet [25,26]. Thus, kink band formation in polycrystals could be the result of a competition between structural effects and microscopic mechanisms that cannot be accounted for within the classical crystal plasticity framework.

Indeed, slip and kink localization modes are strictly equivalent in these models from the constitutive perspective. Yet considering associated dislocation mechanisms, both modes are very different. Indeed, slip bands formation involves only a few very active dislocation sources located in close slip planes whereas kink band formation involves the activation of a considerably larger number of sources aligned along the direction normal to the slip plane. Hence, the two modes are not equivalent regarding dislocation mechanisms. For materials exhibiting strong softening mechanisms intensification of dislocation emission from already active sources is promoted over activation of new sources and thus kink bands formation should be highly unlikely. Kink bands are indeed never reported in observations of deformed irradiated or quench-hardened metals, that undergo such softening mechanisms (dislocation channeling), where slip localization seems to occur only through intense slip bands. Yet, Fig. 11 clearly shows that a state of the art physics based model design for austenitic stainless steel modeling predicts the formation of a large amount of kink bands. Consequently classical crystal plasticity models appear to be fundamentally unable to reproduce accurately localization bands formation in these materials. Fig. 11.

7. Conclusions

We have used a massively parallel FFT solver to study intragranular strain localization induced by a strain softening classical crystal plasticity model. This numerical tool allows to compute realistic three dimensional polycrystalline simulations including full description of complex crystal systems and achieve grid resolutions that allow for a fine description of intragranular localization bands. Our simulations show the formation of an intragranular localization network of narrow bands exhibiting high plastic slip.

We proposed a new qualitative approach to study localized deformation at incipient plasticity in polycrystals. It relies on the systematic analysis of the nature of simulated localization bands based on the processing of equivalent plastic strain and lattice rotation fields. We produced localization maps that where used to accurately identify the slip and kink band populations in the localization network, for both simple bidimensional simulations and realistic three dimensional polycrystals with complex crystal systems. Quantification of band volume fraction and mean plastic strain highlight the distinct mechanical characteristics of simulated slip and kink bands. Because of rotation induced hardening, kink bands tend to widen with increasing loading, and their volume fraction and mean strain level are less sensitive to mesh dependence and softening magnitude.

In agreement with Asaro and Rice's bifurcation analysis, we showed that slip or kink bands localization modes are strictly equivalent for polycrystalline simulations assuming initially homogeneous grains and softening classical crystal plasticity constitutive equations. They only account for strain incompatibility effects on plastic localization mode formation, which translate into a large amount of kink bands in all simulations of softening polycrystals. In physical materials exhibiting strain localization, deformation is mainly associated to one specific mode. For instance anisotropic crystals deform mainly through kink banding, when strongly softening metals through slip banding. Consequently, our work demonstrates that:

- Identification of localization modes when simulating intragranular strain localization is fundamental in order to properly assess the validity of crystal plasticity models, by means of comparison with experimental characterization of bands nature.
- Classical crystal plasticity models, systematically predict comparable amount of slip and kink bands, as they are two equivalent strain localization modes within this framework, in agreement with Asaro and Rice's analysis.
- Slip banding is largely the main deformation mode observed in strongly softening metals, such as hyper-quenched metals or irradiated metals in which kink bands are not reported. Hence, classical crystal plasticity models are fundamentally unable to accurately simulate strain localization in such materials.

Therefore, the use of local crystal plasticity equations can be enriched with a continuum explicitly accounting for a band structure in the material description. For instance, Kumar and Mahesh proposed to model the single crystal as a a laminate stack of homogeneously deforming domains [61]; Zhang and coworkers [62] enriched a finite element classical crystal plasticity model by prescribing material softening within a band structure defined a priori for each slip system, and were able to qualitatively capture the slip band formation in experimental observations.

Alternatively, in order to accurately simulate intragranular strain localization at the continuum scale in softening metals, physical mechanisms that can promote or preclude individually kink or slip band formation need to be accounted for with more complex plasticity theories. For instance, Cosserat plasticity has been shown to break the equivalence of slip and kink modes in the bifurcation analysis associated to slip localization and to postpone or even preclude formation of kink bands in single crystals simulations [13]. Likewise, strain gradient plasticity models based on an energy density associated to the geometrically necessary dislocation (GND) [63] density tensor allow to introduce a distinction between slip and kink bands. The existing finite element or FFT implementations [13,64,65] together with our massively parallel implementation open the way to analyze plastic localization modes in polycrystalline simulations based on strain-gradient softening models to better reproduce accurately slip/kink bands populations.

Appendix A. Integration of classical softening equations used for dislocation channeling modeling

Physics based models for irradiated metals available in the literature [39–45,51] rely on two mechanisms. The first is the hardening effect of the irradiation induced defects in the crystal. The second is the dislocation channeling mechanism: gliding dislocation interactions with irradiation induced defects lead to the progressive annihilation of the defects and thus leading to a strong softening in the areas swept by many dislocations. The set of constitutive equations used by these authors to model these two mechanisms have the same form, and reduce to an exponential

decay law of the critical resolved shear stress, similar to the one used in this work (4), when integrated for the single slip case.

To illustrate this, we rely on the irradiated Zirconium model given in Ref. [41]. According to the dispersed barrier hardening model the increase in resolved shear stress due the radiation induced dislocation loops is expressed by:

$$\Delta\tau_c = \alpha\mu b\sqrt{Nd} \tag{A.1}$$

where μ is the shear modulus, N is the loop density, d is the loop diameter, b the loop Burgers vector and α the loop obstacle strength. The evolution of the loop density is given by the equation:

$$\dot{\rho_l} = -k_B\rho_l[\sum_{s\in B}|\dot{\gamma}_s|] \tag{A.2}$$

where $\rho_l = Nd$, and $s\in B$ denotes the sum over slip systems of the basal plane. During the formation of a dislocation channel, it is reasonable to assume single slip conditions. Eq. (A.2) then reduces to:

$$\dot{\rho_l} = -k_B\rho_l|\dot{\gamma}| \tag{A.3}$$

which after integration yields:

$$\rho_l = \rho_0\exp(-k_B|\gamma|) \tag{A.4}$$

Eq. (A.4) is then reintroduced in Eq. (A.1) to yield the exponential decay in the softening equation:

$$\Delta\tau_c = \alpha\mu b\sqrt{\rho_l} = \alpha\mu b\sqrt{\rho_0}\exp\left(\frac{-k_B|\gamma|}{2}\right) \tag{A.5}$$

Appendix B. Mechanical behavior parameters influence on slip and kink bands

Appendix B.1. Strain-rate sensitivity

Strain localization phenomenon can occur for a large range of temperatures, or can also be associated to local adiabatic heating. This change in temperature will affect material viscosity and could potentially have an influence of strain localization patterns or intensity. To investigate this effect, a complementary study of the impact of strain-rate sensitivity on slip and kink bands has been carried. Strain-rate sensitivity is essentially dependent on the Norton exponent n in the flow rule Eq. (2). Simulations with various values for n in a range going from $n = 2$ to $n = 50$ have been conducted. The results show that the only noticeable effect is that an increased strain-rate sensitivity (low value of n) leads to a small increase of the bands volume fraction. Besides that, in the range of values that we studied (from $n = 2$ to $n = 50$), the localization pattern and band intensity is unchanged when n varies, as can be seen on the figures and localization maps (maps (a) is obtained for $n = 2$, (b) for $n = 50$).

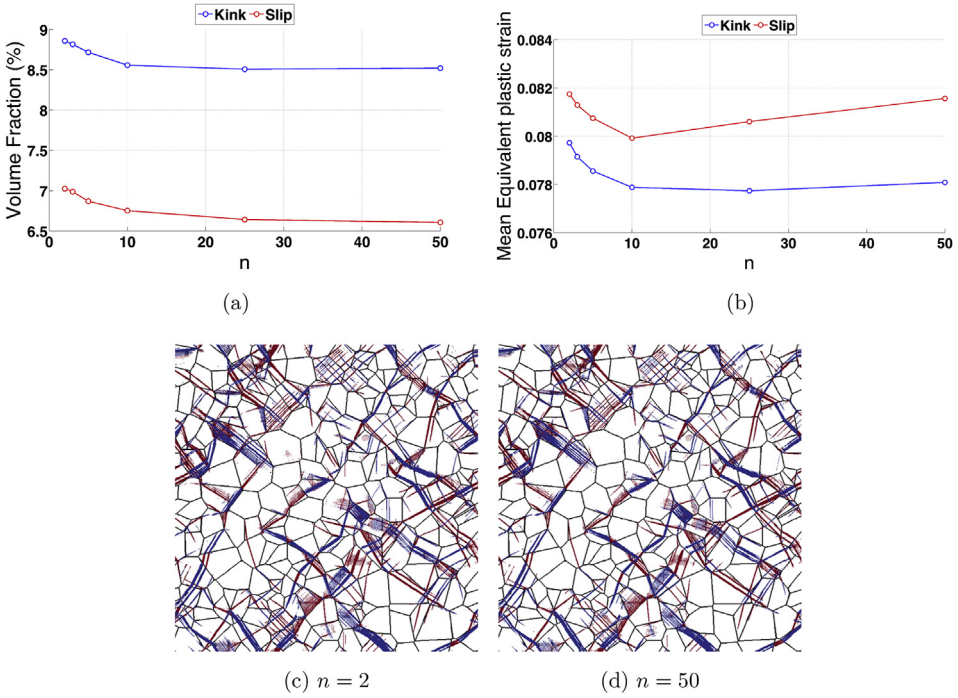

Fig. B.12. Evolution of slip/kink bands volume fraction (a) and mean equivalent plastic strain (b) with Norton exponent n for the 2D polycrystal after 1% overall strain. Associated localization pattern for $n = 2$ (c) and $n = 50$ (d). Grid resolution: 750×750 voxels.

Appendix B.2. Hardening

Asaro and Rice [12] predicted in their bifurcation analysis that slip and kink banding can occur even for a strain-hardening material. They showed that if geometrical softening can overcome material hardening, plastic strain will localize into a slip or a kink band. With a view to investigate if our simulations and localization modes analysis can evidence strain localization in this case, an additional linear hardening term has been added to the CRSS equation:

$$\tau_c^\alpha = \tau_{c_i}^\alpha - \Delta\tau^\alpha\left(1 - \exp\left(-\frac{\gamma_{cum}^\alpha}{\gamma_0^\alpha}\right)\right) + H\cdot\gamma_{cum}^\alpha \qquad \text{(B.1)}$$

where H is the linear hardening modulus.

A simulation has been conducted with the 2D polycrystalline unit cell, the material coefficients of Table 1, except $\Delta\tau$, in order to model a purely linear hardening material by setting $\Delta\tau = 0$ MPa. A small hardening modulus has been chosen, $H = 40$ MPa, for the purpose of allowing geometrical softening to quickly overcome hardening. As predicted by Asaro and Rice, we observe strain localization in our simulation, as shown on Fig. B.13(e). Localization bands are logically thicker than in the purely softening simulations (Fig. 5), but the same localization pattern is observed. The same grains exhibit the same localization modes in the softening and the slightly hardening simulations.

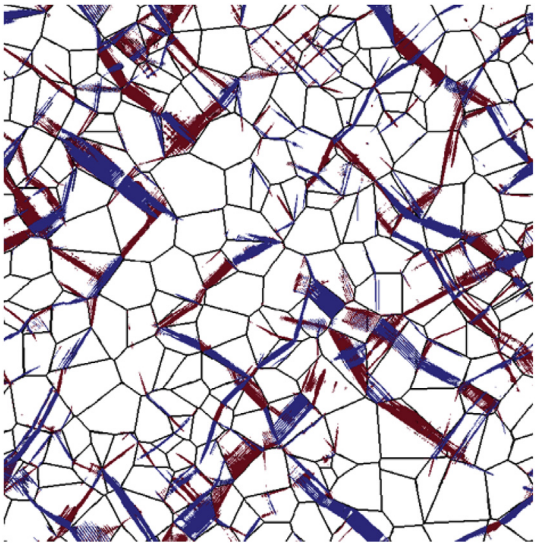

Fig. B.13. Localization map obtain for the 2D polycrystal after 1% overall strain after a purely hardening simulation: $H = 40$ MPa, $\Delta\tau = 0$ MPa. Grid resolution: 750×750 voxels.

References

[1] B. Jaoul, Etude de la plasticité et application aux métaux, Les Presses - Mines ParisTech, 1964.

[2] H. Neuhäuser, in: F.R.N. Nabarro (Ed.), Dislocation in Solids, vol. 6, Holland Publishing Company, 1983, pp. 319–440.

[3] C. Wilson, J. Burg, J. Mitchell, The origin of kinks in polycrystalline ice, Tectonophysics 127 (1986) 27–48, https://doi.org/10.1016/0040-1951(86)90077-6.

[4] M. Montagnat, J.R. Blackford, S. Piazolo, L. Arnaud, R.A. Lebensohn, Measurements and full-field predictions of deformation heterogeneities in ice, Earth Planet. Sci. Lett. 305 (2011) 153–160, https://doi.org/10.1016/j.epsl.2011.02.050.

[5] P. Mansuy, A. Philip, J. Meyssonier, Localization of deformation in polycrystalline ice, J. Phys. 11 (2001) 267–274. https://doi.org/10.1051/jp4:2001433.

[6] K. Hagihara, T. Mayama, M. Honnami, M. Yamasaki, H. Izuno, T. Okamoto, T. Ohashi, T. Nakano, Y. Kawamura, Orientation dependence of the deformation kink band formation behavior in Zn single crystals, Int. J. Plast. 77 (2016) 174–191, https://doi.org/10.1016/j.ijplas.2015.10.005.

[7] K. Hagihara, T. Okamoto, M. Yamasaki, Y. Kawamura, T. Nakano, Electron backscatter diffraction pattern analysis of the deformation band formed in the Mg-based long-period stacking ordered phase, Scripta Mater. 117 (2016) 32–36, https://doi.org/10.1016/j.scriptamat.2016.02.016.

[8] W. Crone, T. Shield, Experimental study of the deformation near a notch tip in copper and copper-beryllium single crystals, J. Mech. Phys. Solids 49 (2001) 2819–2938. https://doi.org/10.1016/S0022-5096(01)00080-1.

[9] J.W. Kysar, C.L. Briant, Crack tip deformation fields in ductile single crystals, Acta Mater. 50 (2002) 2367–2380, https://doi.org/10.1016/S1359-6454(02)00070-8.

[10] S.D. Patil, R. Narasimhana, R.K. Mishra, Observation of kink shear bands in an aluminium single crystal fracture specimen, Scripta Mater. 61 (2009) 465–468, https://doi.org/10.1016/j.scriptamat.2009.04.043.

[11] Y. Zheng, W. Zeng, Y. Wang, S. Zhang, Kink deformation in a beta titanium alloy at high strain rate, Mater. Sci. Eng. A 702 (2017) 218–224, https://doi.org/10.1016/j.msea.2017.07.015.

[12] R. Asaro, J. Rice, Strain localization in ductile single crystals, J. Mech. Phys. Solids 25 (1977) 309–338, https://doi.org/10.1016/0022-5096(77)90001-1.

[13] S. Forest, Modeling slip, kink and shear banding in classical and generalized single crystal plasticity, Acta Mater. 46 (1998) 3265–3281, https://doi.org/10.1016/S1359-6454(98)00012-3.

[14] R. Lebensohn, M. Montagnat, P. Mansuy, P. Duval, J. Meysonnier, A. Philip, Modeling viscoplastic behavior and heterogeneous intracrystalline deformation of columnar ice polycrystals, Acta Mater. 57 (2009) 1405–1415, https://doi.org/10.1016/j.actamat.2008.10.057.

[15] Y. Kimura, R. Ueta, K. Shizawa, Dislocation-based crystal plasticity FE analysis for kink band formation in Mg-based LPSO phase considering higher-order stress, Procedia Manuf. 15 (2018) 1825–1832, https://doi.org/10.1016/j.promfg.2018.07.208.

[16] A. Korbel, M. Szczerba, Strain hardening of copper single crystals at high strains and dynamical recovery processes, Acta Metall. 30 (1981) 1961–1982.

[17] A. Korbel, M. Szczerba, Strain softening and instability of plastic flow in cu-al single crystals, Acta Metall. 35 (1986) 1129–1135.

[18] A. Churchman, The yield phenomena, kink bands and geometric softening in titanium crystals, Acta Metall. 3 (1955) 22–29, https://doi.org/10.1016/0001-6160(55)90006-7.

[19] Y. Estrin, L. Kubin, Local strain hardening and nonuniformity of plastic deformation, Acta Metall. 34 (1986) 2455–2464. https://doi.org/10.1016/0001-6160(86)90148-3.

[20] Y. Brechet, G. Canova, L. Kubin, Static versus propagative strain localisations, Scripta Metall. Mater. 29 (1993) 1165–1170, https://doi.org/10.1016/0956-716X(93)90103-Y.

[21] D. Ulmer, C. Altstetter, Hydrogen-induced strain localization and failure of austenitic stainless steels at high hydrogen concentrations, Acta Metall. Mater. 39 (1991) 1237–1248. https://doi.org/10.1016/0956-7151(91)90211-I.

[22] I. Aubert, N. Saintier, J. Olive, Crystal plasticity computation and atomic force microscopy analysis of the internal hydrogen-induced slip localization on polycrystalline stainless steel, Scripta Mater. 66 (2012) 698–701, https://doi.org/10.1016/j.scriptamat.2012.01.019.

[23] J. Sharp, Correlation between cleared channels and surface slip steps in neutron irradiated copper crystals, Radiat. Eff. 14 (1972) 71–75, https://doi.org/10.1080/00337577208230474.

[24] D. Edwards, B. Singh, J. Bilde-Sorensen, Initiation and propagation of cleared channels in neutron-irradiated pure copper and a precipitation hardened CuCrZr alloy, J. Nucl. Mater. 342 (2005) 164–178, https://doi.org/10.1016/j.jnucmat.2005.04.001.

[25] F. Onimus, I. Monnet, J. Béchade, C. Prioul, P. Pilvin, A statistical TEM investigation of dislocation channeling mechanism in neutron irradiated zirconium alloys, J. Nucl. Mater. 328 (2004) 165–179, https://doi.org/10.1016/j.jnucmat.2004.04.337.

[26] L. Fournier, A. Serres, Q. Auzoux, D. Leboulch, G. Was, Proton irradiation effect on microstructure, strain localization and iodine-induced stress corrosion cracking in Zircaloy-4, J. Nucl. Mater. 384 (2009) 38–47, https://doi.org/10.1016/j.jnucmat.2008.10.001.

[27] M. Sauzay, K. Bavard, W. Karlsen, TEM observations and finite element modelling of channel deformation in pre-irradiated austenitic stainless steels - interactions with free surfaces and grain boundaries, J. Nucl. Mater. 406 (2010) 152–165, https://doi.org/10.1016/j.jnucmat.2010.01.027.

[28] T. Byun, N. Hashimoto, K. Farrell, E. Lee, Characteristics of microscopic strain localization in irradiated 316 stainless steels and pure vanadium, J. Nucl. Mater. 349 (2006) 251–264, https://doi.org/10.1016/j.jnucmat.2005.10.011.

[29] T. Byun, N. Hashimoto, K. Farell, Deformation mode map of irradiated 316 stainless steel in true stress-dose space, J. Nucl. Mater. 351 (2006) 303–315, https://doi.org/10.1016/j.jnucmat.2006.02.033.

[30] K. Field, M.N. Gussev, J. Busby, Microstructural characterization of deformation localization at small strains in a neutron-irradiated 304 stainless steel, J. Nucl. Mater. 452 (2014) 500–508, https://doi.org/10.1016/j.jnucmat.2014.05.053.

[31] N. Hashimoto, T. Byun, K. Farell, S. Zinkle, Deformation microstructure of neutron-irradiated pure polycrystalline vanadium, J. Nucl. Mater. 336 (2005) 225–232, https://doi.org/10.1016/j.jnucmat.2004.09.017.

[32] T. Mori, M. Meshii, Plastic deformation of quench-hardened aluminium single crystals, Acta Metall. 17 (1969) 167–175, https://doi.org/10.1016/0001-6160(69)90137-0.

[33] M. Bapna, M. Meshii, Deformation of quench-hardened gold crystals, Mater. Sci. Eng. 16 (1974) 181–191. https://doi.org/10.1016/0025-5416(74)90152-9.
[34] F. Onimus, L. Dupuy, F. Mompiou, In situ TEM observations of interactions between gliding dislocations and prismatic loops in Zr-ion irradiated zirconium alloys, Prog. Nucl. Energy 57 (2012) 77–85, https://doi.org/10.1016/j.pnucene.2011.10.005.
[35] M. Lai, C. Tasan, D. Raabe, Deformation mechanism of omega-enriched Ti–Nb-based gum metal : dislocation channeling and deformation induced omega–beta transformation, Acta Mater. 100 (2015) 290–300. https://doi.org/10.1016/j.actamat.2015.08.047.
[36] D. Rodney, Atomic-scale modeling of clear band formation in FCC metals, Nucl. Instrum. Methods Phys. Res. B 225 (2005) 100–110, https://doi.org/10.1016/j.nimb.2004.10.029.
[37] T. Nogaret, D. Rodney, M. Fivel, C. Robertson, Clear-band formation simulated by dislocation dynamics: role of helical turns and pile-ups, J. Nucl. Mater. 380 (2008) 22–29, https://doi.org/10.1016/j.jnucmat.2008.07.001.
[38] A. Arsenlis, M. Rhee, G. Hommes, R. Cook, J. Marian, A dislocation dynamics study of the transition from homogeneous to heterogeneous deformation in irradiated body-centered cubic iron, Acta Mater. 60 (2012) 3748–3757, https://doi.org/10.1016/j.actamat.2012.03.041.
[39] A. Arsenlis, B.D. Wirth, M. Rhee, Dislocation density-based constitutive model for the mechanical behaviour of irradiated Cu, Phil. Mag. 84 (34) (2004) 3617–3635, https://doi.org/10.1080/14786430412331293531.
[40] S. Krishna, A. Zamiri, S. De, Dislocation and defect density-based micro-mechanical modeling of the mechanical behavior of FCC metals under neutron irradiation, Phil. Mag. 90 (30) (2010) 4013–4025, https://doi.org/10.1080/14786435.2010.502150.
[41] F. Onimus, J.-L. Bechade, A polycrystalline modeling of the mechanical behavior of neutron irradiated zirconium alloys, J. Nucl. Mater. 384 (2009) 163–174, https://doi.org/10.1016/j.jnucmat.2008.11.006.
[42] N. Barton, A. Arsenlis, J. Marian, A polycrystal plasticity model of strain localization in irradiated iron, J. Mech. Phys. Solids 61 (2013) 341–351, https://doi.org/10.1016/j.jmps.2012.10.009.
[43] A. Patra, D. McDowell, Crystal plasticity-based constitutive modelling of irradiated BCC structures, Phil. Mag. 92 (7) (2012) 861–887, https://doi.org/10.1080/14786435.2011.634855.
[44] X. Xiao, D. Song, J. Xue, H. Chu, H. Duan, A size-dependent tensorial plasticity model for FCC single crystals with irradiation, Int. J. Plast. 65 (2015) 152–167, https://doi.org/10.1016/j.ijplas.2014.09.004.
[45] J. Hure, S.E. Shawish, L. Cizelj, B. Tanguy, Intergranular stress distributions in polycrystalline aggregates, J. Nucl. Mater. 476 (2016) 231–242, https://doi.org/10.1016/j.jnucmat.2016.04.017.
[46] M. Zhang, F. Bridier, P. Villechaise, J. Mendez, D. McDowell, Simulation of slip band evolution in duplex Ti-6Al-4V, Acta Mater. 58 (2010) 1087–1096, https://doi.org/10.1016/j.actamat.2009.10.025.
[47] T. Erinosho, F. Dunne, Strain localization and failure in irradiated zircaloy with crystal plasticity, Int. J. Plast. 71 (2015) 170–194, https://doi.org/10.1016/j.ijplas.2015.05.008.
[48] A. Patra, D. McDowell, Continuum modelling of localized deformation in irradiated bcc materials, J. Nucl. Mater. 432 (2013) 414–427, https://doi.org/10.1016/j.jnucmat.2012.08.021.
[49] A. Patra, D. McDowell, Crystal plasticity investigation of the microstructural factors influencing dislocation channeling in a model irradiated bcc material, Acta Mater. 110 (2016) 364–376, https://doi.org/10.1016/j.actamat.2016.03.041.
[50] J. Mandel, Equations constitutives et directeurs dans les milieux plastiques et viscoplastiques, Int. J. Solids Struct. 9 (1973) 725–740, https://doi.org/10.1016/0020-7683(73)90120-0.
[51] C. Ling, B. Tanguy, J. Besson, S. Forest, F. Latourte, Void growth and coalescence in triaxial stress fields in irradiated FCC single crystals, J. Nucl. Mater. 492 (2017) 157–170, https://doi.org/10.1016/j.jnucmat.2017.04.013.
[52] H. Moulinec, P. Suquet, A numerical method for computing the overall response of nonlinear composites with complex microstructure, Comput. Methods Appl. Mech. Eng. 157 (1998) 69–94, https://doi.org/10.1016/S0045-7825(97)00218-1.
[53] F. Willot, Fourier-based schemes for computing the mechanical response of composites with accurate local fields, Compt. Rendus Mec. 343 (2015) 232–245. https://doi.org/10.1016/j.crme.2014.12.005.
[54] M. Schneider, D. Merkert, M. Kabel, FFT-based homogenization for micro-structures discretized by linear hexahedral elements, Int. J. Numer. Methods Eng. 109 (2017) 1461–1489, https://doi.org/10.1002/nme.5336.
[55] D. Anderson, Iterative procedures for nonlinear integral equations, J. Assoc. Comput. Mach. 12 (1965) 547–560, https://doi.org/10.1145/321296.321305.
[56] H. Walker, P. Ni, Anderson acceleration for fixed-point iterations, SIAM J. Numer. Anal. 49 (2011) 1715–1735. https://doi.org/10.1137/10078356X.
[57] I. Ramière, T. Helfer, Iterative residual-based vector methods to accelerate fixed point iterations, Comput. Math. Appl. 70 (2015) 2210–2226. https://doi.org/10.1016/j.camwa.2015.08.025.
[58] T. Helfer, B. Michel, J.-M. Proix, M. Salvo, J. Sercombe, Introducing the open-source MFront code generator: application to mechanical behaviours and material knowledge management within the PLEIADES fuel element modelling platform, Comput. Math. Appl. 70 (2015) 994–1023. https://doi.org/10.1016/j.camwa.2015.06.027.
[59] C. Ling, B. Tanguy, J. Besson, S. Forest, F. Latourte, E. Bosso, An elastovisco-plastic model for porous single crystals at finite strains and its assessment based on unit cell simulations, Int. J. Plast. 84 (2016) 58–87. https://doi.org/10.1016/j.ijplas.2016.05.001.
[60] S. Flouriot, S. Forest, G. Cailletaud, A. Köster, L. Rémy, B. Burgardt, V. Gros, S. Mosset, J. Delautre, Strain localization at the crack tip in single crystal CT specimens under monotonous loading: 3D finite element analyses and application to nickel-base superalloys, Int. J. Fract. 124 (2003) 44–77, https://doi.org/10.1023/B:FRAC.0000009300.70477.ba.
[61] M.A. Kumar, S. Mahesh, Banding in single crystals during plastic deformation, Int. J. Plast. 36 (2012) 15–33. https://doi.org/10.1016/j.ijplas.2012.03.008.
[62] M. Zhang, F. Bridier, P. Villechaise, J. Mendez, D. McDowell, Simulation of slip band evolution in duplex ti-6al-4v, Acta Mater. 58 (2010) 1087–1096, https://doi.org/10.1016/j.actamat.2009.10.025.
[63] M.E. Gurtin, A gradient theory of single-crystal viscoplasticity that accounts for geometrically necessary dislocations, J. Mech. Phys. Solids 50 (2002) 5–32. https://doi.org/10.1016/S0022-5096(01)00104-1.
[64] N. Cordero, S. Forest, E.P. Busso, Generalised continuum modelling of grain size effects in polycrystals, Compt. Rendus Mec. 340 (2012) 261–274, https://doi.org/10.1016/j.crme.2012.02.009.
[65] A. N. Ricardo A. Lebensohn, Numerical implementation of non-local polycrystal plasticity using fast fourier transforms, J. Mech. Phys. Solids 97 (2016) 333–351. https://doi.org/10.1016/j.jmps.2016.03.023.